communications biology

Article

https://doi.org/10.1038/s42003-024-06655-y

Dental pulp stem cells-derived cannabidiol-treated organoid-like microspheroids show robust osteogenic potential via upregulation of WNT6

Fangqi Liu[1], Qingqing Wu[1], Qianwen Liu[1], Bo Chen[1], Xintong Liu[2,3], Janak L. Pathak[1] ✉, Nobumoto Watanabe[2,3] & Jiang Li[1] ✉

Dental pulp stem cells (DPSC) have shown osteogenic and bone regenerative potential. Improving the in situ bone regeneration potential of DPSC is crucial for their application as seed cells during bone defect reconstruction in clinics. This study aimed to develop DPSC-derived organoid-like microspheroids as effective seeds for bone tissue engineering applications. DPSC osteogenic microspheroids (70 µm diameter) were cultured in a polydimethylsiloxane-mold-based agarose-gel microwell-culture-system with or without cannabidiol (CBD)-treatment. Results of in vitro studies showed higher osteogenic differentiation potential of microspheroids compared with 2D-cultured-DPSC. CBD treatment further improved the osteogenic differentiation potential of microspheroids. The effect of CBD treatment in the osteogenic differentiation of microspheroids was more pronounced compared with that of CBD-treated 2D-cultured-DPSC. Microspheroids showed a higher degree of bone regeneration in nude mice calvarial bone defect compared to 2D-cultured-DPSC. CBD-treated microspheroids showed the most robust in situ bone regenerative potential compared with microspheroids or CBD-treated 2D-cultured-DPSC. According to mRNA sequencing, bioinformatic analysis, and confirmation study, the higher osteogenic potential of CBD-treated microspheroids was mainly attributed to WNT6 upregulation. Taken together, DPSC microspheroids have robust osteogenic potential and can effectively translate the effect of in vitro osteoinductive stimulation during in situ bone regeneration, indicating their application potential during bone defect reconstruction in clinics.

Development of functional bone constructs using mesenchymal stem cells (MSCs), biomimetic biomaterial scaffolds, and growth factors are current strategies of bone tissue engineering[1–3]. Autologous MSCs obtained from different anatomical sites such as bone marrow, adipose tissue, and dental pulp are commonly used in clinics to repair large-sized bone defects[4–6]. Dental pulp stem cells (DPSCs), as easily accessible MSCs, can be extracted from orthodontic teeth or wisdom teeth in a non-invasive way[4,7]. Due to easy accessibility, high proliferation ability, and multilineage differentiation properties, DPSCs are considered potential seeds for orthopedic and oral maxillofacial reconstruction as well as for dental tissue regeneration[8–10]. However, the clinical outcomes of DPSC-based bone tissue-engineering strategies are still not satisfactory.

During stem cell-based bone tissue engineering, in situ seeded MSCs should proliferate and survive long enough to differentiate in osteoblasts as well as to release the growth factors and chemokines to influence the cells of surrounding tissues such as endothelial cells and macrophages[11,12]. However, the grafted seed cells can survive only a few days in vivo fading effective bone regeneration[13,14]. To fulfill the need for more effective seeds, 3D culture

[1]School and Hospital of Stomatology, Guangdong Engineering Research Center of Oral Restoration and Reconstruction, Guangzhou Key Laboratory of Basic and Applied Research of Oral Regenerative Medicine, Guangzhou Medical University, Guangzhou, 510182, China. [2]Chemical Biology Research Group, RIKEN Center for Sustainable Resource Science, Wako, Saitama, 351-0198, Japan. [3]Bio-Active Compounds Discovery Unit, RIKEN Center for Sustainable Resource Science, Wako, Saitama, 351-0198, Japan. ✉e-mail: J.pathak@gzhmu.edu.cn; ljiang@gzhmu.edu.cn

technologies including MSC-derived cell sheet aggregates[15], micro-tissues, spheroids[16], and organoids[17,18] have been developed that provide superior nutrient, oxygen gradients, cell–cell interaction, and matrix deposition required for tissue regeneration[19–21]. The architecture and organization of cells in a 3D environment differ from those in a 2D environment, which can affect cell behavior and drug response[22,23]. 3D-printed porous bone grafts are mainly designed with pore sizes 200–500 μm[24]. Cell aggregates/spheroids produced by the conventional 3D culture techniques fail to control the size and cell numbers which causes cell necrosis and difficulties in homogenous seeding of aggregates/spheroids throughout the microporous scaffolds[13,25]. Therefore, the development of MSCs-derived organoid-like biomimetic osteogenic microspheroids (with <100 μm size) is crucial for homogeneous loading in microporous bone grafts during the surgical procedure[26].

Inducing the osteogenic potential of cell aggregates/spheroids during bone defect healing is still a challenge. In situ application of growth factors or osteoinductive agents improves bone regeneration but poses the risk of adverse effects. The development of MSCs-derived organoid-like microspheroids that can effectively translate in vitro osteoinductive stimulation during in vivo grafting could avoid the direct in vivo application of osteoinductive agent-related adverse effects. Natural products have shown promising potential to promote bone regeneration[27,28]. Cannabidiol (CBD), a major non-psychotropic constituent of *Cannabis sativa*, promotes the osteogenic differentiation of DPSC[29]. CBD has certain biological activities required for bone tissue engineering such as anti-inflammatory[30], antioxidant[31], chemotactic[32], angiogenic, and osteogenic[33] properties. Although CBD is a relatively safe drug for in vivo application, it might still exert local and systemic adverse effects[34,35]. Based on these facts, we choose CBD as a potential osteoinductive agent to test in vitro osteoinductive stimulation translation ability of DPSC microspheroids during in situ bone regeneration.

This study aimed to develop DPSC-based organoid-like osteogenic microspheroids that can be easily injected as effective seeds during bone tissue engineering. We also aim to investigate the in vitro osteoinductive stimulation translation ability of DPSC microspheroids during in situ bone regeneration using CBD as an osteoinductive drug model. We developed organoid-like DPSC microspheroids of 70 μm size using the self-assembled microwell culture technique. Microspheroids were cultured with the osteogenic medium (OM) in the presence or absence of CBD for 14 days. In vitro osteogenic differentiation and in situ bone regeneration potentials of CBD-treated microspheroids, microspheroids, CBD-treated 2D-expanded-DPSC, and 2D-expanded-DPSC were compared. The mechanism of CBD-induced osteogenic potential of the DPSC microspheroids was further investigated.

Results

Isolation and characterization of DPSC

DPSC started to crawl out from enzyme-digested dental pulp tissues after 5 days of culture. The cells around the tissue mass were adherent to the culture dish surface and proliferated gradually, forming the appearance of cell colonies (Fig. 1A). The DPSC showed fibroblast-like morphology and active proliferation capacity during passage 3 (Fig. 1B). DPSC were positive for MSC surface markers, including CD29, CD44, CD90, CD73, and CD105

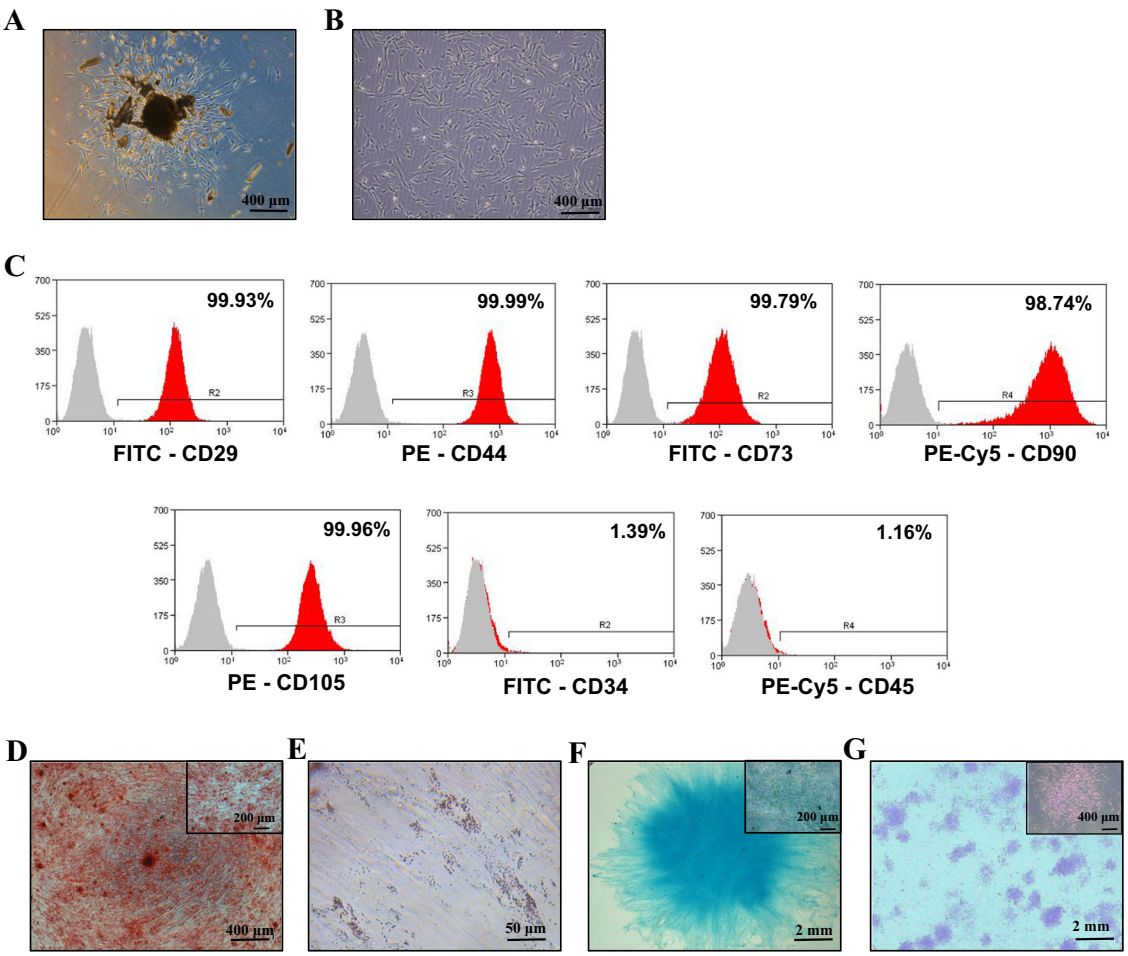

Fig. 1 | Characterization of DPSC. Primary stem cells from human permanent teeth P0: passage 0 (**A**) and P3: passage 3 (**B**). **C** Detection of cell surface markers in DPSC by flow cytometry. Analysis of osteogenic, adipogenic, and chondrogenic differentiation potential of DPSC using Alizarin red (**D**), Oil red O (**E**), and Alcian blue staining (**F**), respectively. **G** Crystal violet stained DPSC colonies at day 7 of colony formation assay.

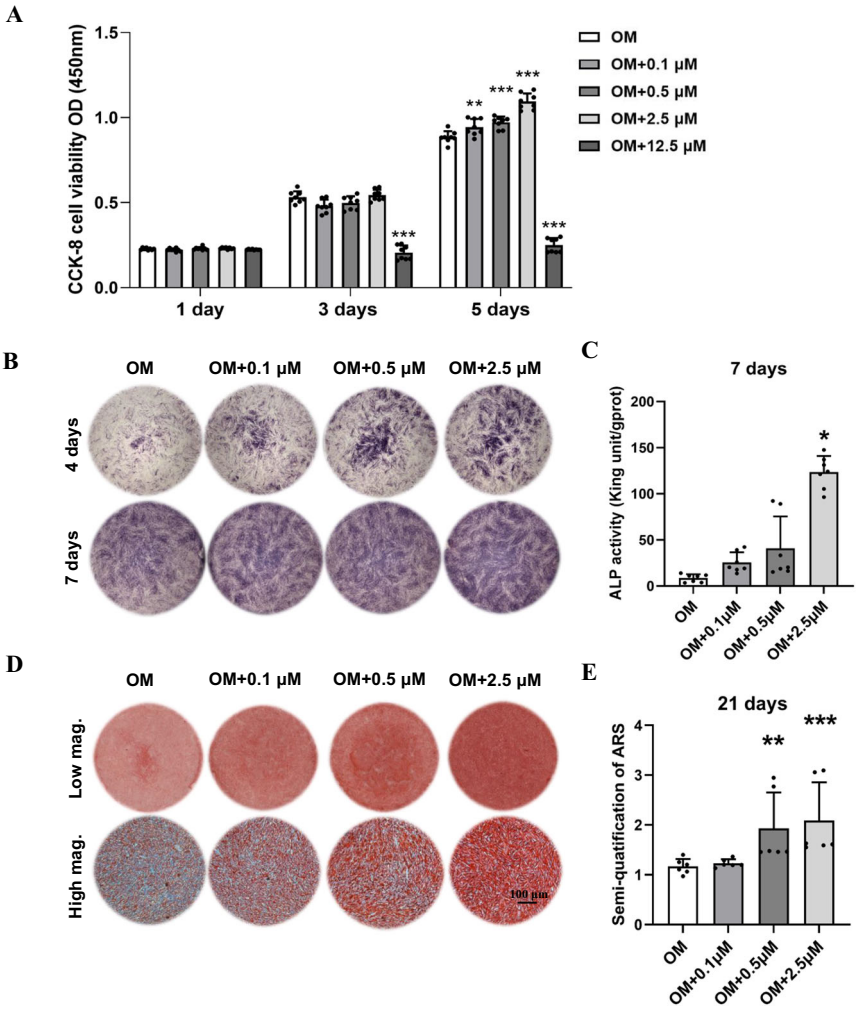

Fig. 2 | Effect of CBD on cell proliferation and osteogenic differentiation of DPSC in vitro. **A** Effect of 0.1, 0.5, 2.5, and 12.5 μM of CBD on the proliferation of DPSC ($n = 6$). ALP staining (**B**) and alizarin red staining (**D**) of DPSC cultured with CBD (0, 0.1, 0.5, and 2.5 μM). **C** ALP activity of DPSC cultured with CBD ($n = 4$). **E** Quantification of mineralized matrix in DPSC cultured with CBD ($n = 4$). The data are presented as mean ± SD. Significant difference compared with the respective control group, $^{*}P < 0.05$, $^{**}P < 0.01$, and $^{***}P < 0.001$. OM osteogenic medium.

and negative for hematopoietic cell markers, such as CD34, and CD45 (Fig. 1C and Supplementary Fig. 1). In addition, DPSC showed robust multilineage differentiation potential as indicated by osteogenic differentiation by alizarin red staining (Fig. 1D), adipogenic differentiation by Oil red O staining (Fig. 1E), and chondrogenic differentiation by Alcian blue staining (Fig. 1F). Lastly, DPSC presented apparent colony-forming capacity at 7 days (Fig. 1G). These results imply the DPSC isolated in this study is a pure source of MSCs.

CBD (2.5 μM) promoted osteogenic differentiation of DPSC in vitro

CBD at concentrations of 0.1, 0.5, and 2.5 μM did not show cytotoxicity towards DPSC at days 1, 3, and 5 of culture. These concentrations of CBD even promoted DPSC proliferation on day 5. However, CBD at a concentration of 12.5 μM caused a significant decrease in cell viability on days 3 and 5, indicating the high dose-dependent cytotoxicity (Fig. 2A). CBD at concentrations of 0.1, 0.5, and 2.5 μM increased alkaline phosphatase (ALP) production by DPSC at day 3 and 7 of culture. Among these three concentrations, CBD 2.5 μM showed the highest effect on ALP production at both time points. This result was also observed in the ALP activity of DPSC on day 7 (Fig. 2B, C). Moreover, CBD at concentrations of 0.1, 0.5, and 2.5 μM promoted matrix mineralization of DPSC at 21 days of culture as indicated by the alizarin red staining and quantification (Fig. 2D, E). Our results indicate 2.5 μM of CBD as an optimal dose for inducing the osteogenic potential of DPSC, and this dose was used for further experiments in this study. To detect the influence of serum-free culture medium, we cultured DPSC in complete osteogenic medium and serum-free osteogenic medium and then examined the expression of osteogenic-related gene. Both groups showed similar expression patterns of osteogenic differentiation markers (Supplementary Fig. 2A).

Microspheroids development and characterization

The polydimethylsiloxane (PDMS) mold with uniform pillars is shown in Fig. 3A. The schematic images of PDMS mold-based agarose-gel microwells and the DPSC microspheres formation in microwells are shown in Fig. 3B, C. After osteogenic induction and with or without CBD treatment, the cytoskeletal actin was stained with tetramethyl rhodamine isothiocyanate (TRITC)-labeled phalloidin and 4′,6-diamidino-2-phenylindole (DAPI). The significant red fluorescent intensity indicated the compaction of microspheroids with actin cytoskeleton by the formation of dense stress fibers over time (Fig. 3D, Supplementary Movie 1, 2). Most cells in the microspheroids were viable (Fig. 3E, Supplementary Movie 3, 4). We also measured the diameter of microspheroids of DPSC during culture. The size of microspheroids decreased over time (Fig. 3F). CBD-treated microspheroids with around 70 μm diameter and active viable cells were successfully developed.

CBD treatment robustly induced osteogenic markers expression in microspheroids

Microspheroids showed robustly higher expression of bone morphogenetic protein 2 (BMP2), runt-related transcription factor 2 (RUNX2), and osteocalcin (OCN) at day 7 compared with DPSC. CBD-treated DPSC or microspheroids showed an increasing trend in the expression of osteogenic markers RUNX2, OCN, and osteopontin (OPN) at day 7. Interestingly,

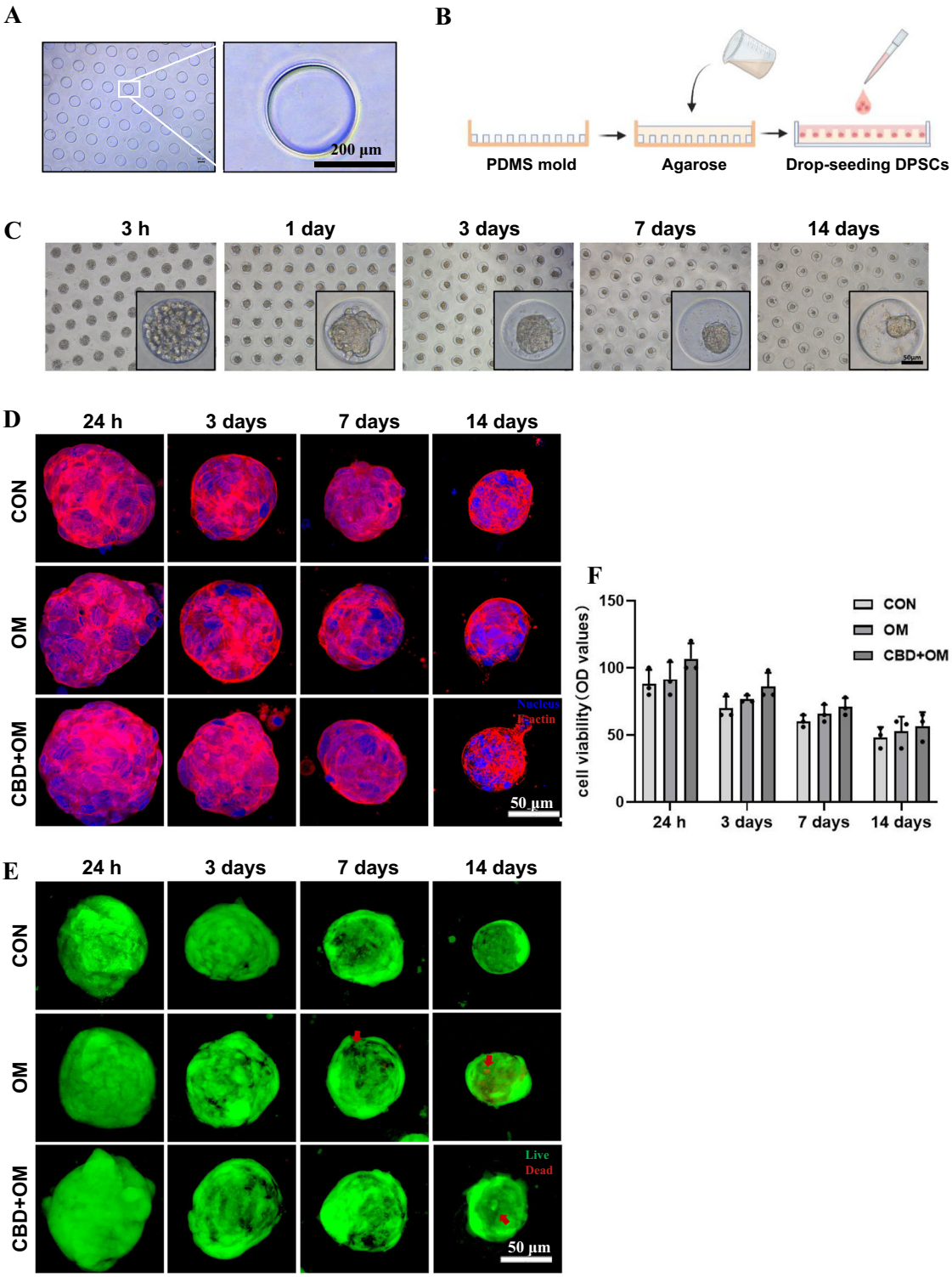

Fig. 3 | Microspheroids development in microwell method. A PDMS mold with uniform microwells. **B** The schematic presentation of agarose microwells on PDMS and the microspheroids formation in microwells. **C** Representative bright-field images of DPSC to microspheroids in a time-dependent manner. Representative confocal z-projection images of cell cytoskeleton in microspheroids stained by Phalloidin actin (**D**), and Live/Dead cells in microspheroids stained by Calcein AM/PI. Red arrows were pointed to the dead cells (**E**). **F** The diameter of microspheroids over time. Scale bar 50 μm. The data are presented as mean ± SD ($n = 3$). OM osteogenic medium.

CBD-treated microspheroids showed higher expression of BMP2, RUNX2, and OCN at day 7 compared with CBD-treated DPSC. Microspheroids showed an increasing trend in ALP, BMP2, RUNX2, OCN, and OPN expression at day 14 compared with DPSC. Similarly, CBD-treated DPSC also showed an increasing trend in ALP, BMP2, RUNX2, OCN, and OPN expression at day 14 compared with DPSC. CBD-treated microspheroids showed robustly higher expression of ALP, BMP2, OCN, and OPN at day 14 compared with microspheroids or CBD-treated DPSC. CBD-treated microspheroids also showed higher expression of RUNX2 at day 14 compared with CBD-treated DPSC (Fig. 4A, B). On day 14, Western blot

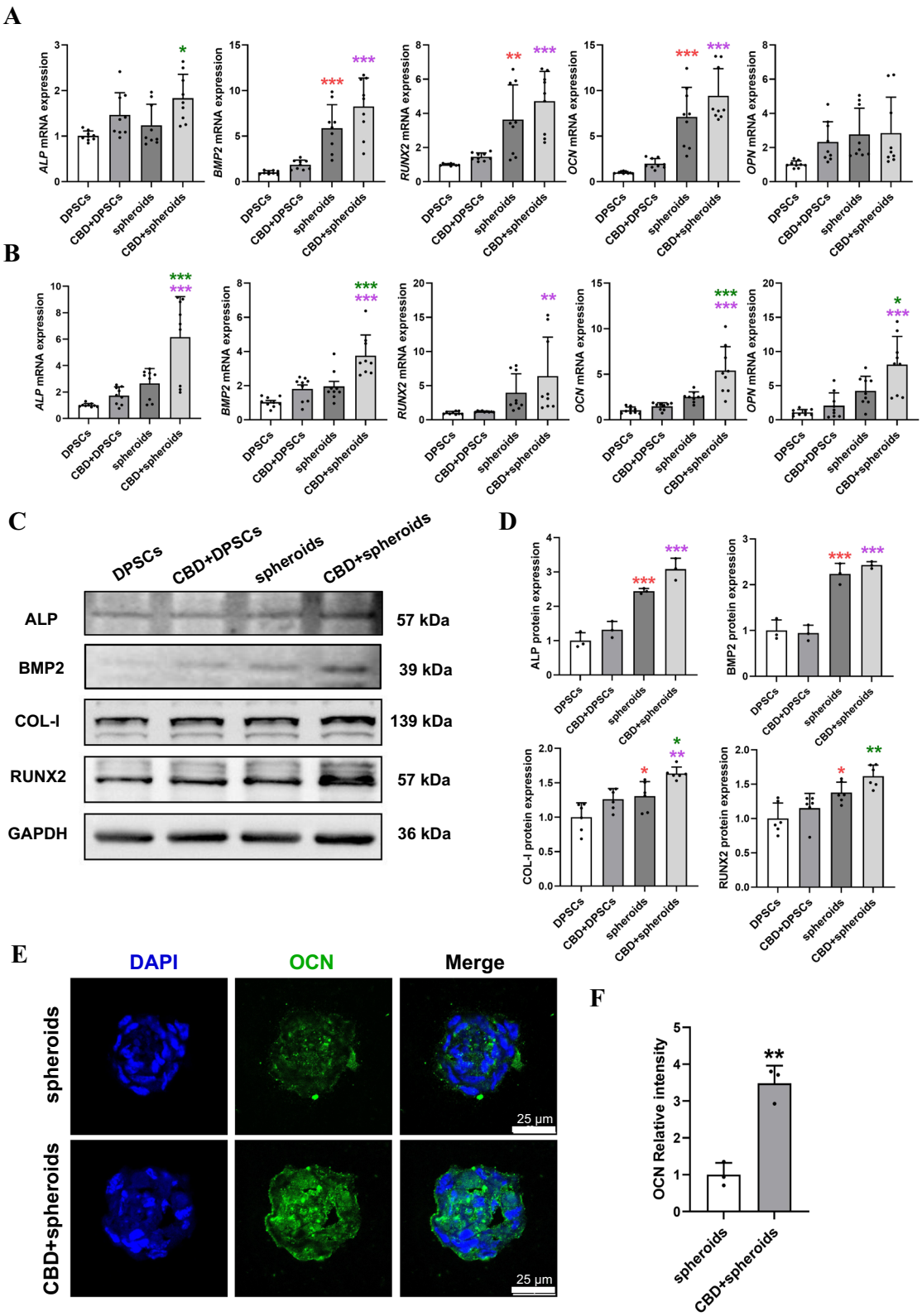

Fig. 4 | CBD (2.5 μM) induced osteogenic markers' expression in microspheroids. ALP, BMP2, RUNX2, OCN, and OPN mRNA expression at day 7 (**A**) and at day 14 (**B**). **C** Representative western blots of ALP, BMP2, COL-1, and RUNX2 expression at day 14 and quantification (**D**). **E** The images of the frozen sections obtained from microspheroids cultured at 14 days under osteogenic medium with or without CBD stained with immunofluorescence and **F** quantification. Data were presented as the mean ± SD ($n = 3$). Significant difference compared different groups, $^{*}P < 0.05$, $^{**}P < 0.01$, and $^{***}P < 0.001$; compared between DPSC and CBD+DPSC groups in blue; compared between DPSC and spheroids groups in red; compared between spheroids and CBD+spheroids groups in green; compared between CBD+DPSC and CBD+spheroids groups in purple.

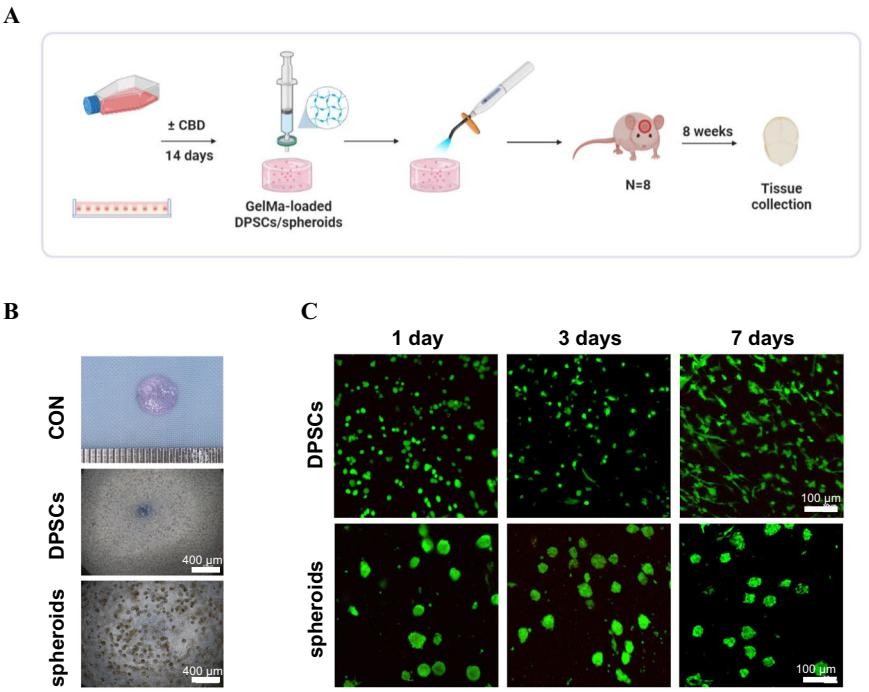

Fig. 5 | Preparation of DPSC or microspheroids loaded GelMA hydrogel constructs for in vivo grafting. The schematic illustration of cell-loaded GelMA hydrogels preparation in vitro and subsequent in vivo construct grafted groups (**A**). **B** The images of the constructs of DPSC-loaded GelMA hydrogels and spheroids-loaded GelMA hydrogels. **C** Images of confocal microscopy showing DPSC or microspheroids viability in GelMA hydrogels assessed using Live/Dead assay.

analysis showed more protein expression of ALP, BMP2, COL-I, and RUNX2 in microspheroids compared with DPSC. CBD-treated microspheroids showed higher protein expression of ALP, BMP2, COL-I, and RUNX2 compared with CBD-treated DPSC. Meanwhile, CBD-treated microspheroids also showed higher protein expression of COL-I compared with microspheroids. (Fig. 4C, D and Supplementary Fig. 4A).

Immunofluorescence imaging and quantification showed higher expression of OCN in CBD-treated microspheroids compared with microspheroids at day 14 (Fig. 4E, F). Our results indicate a higher osteogenic potential of microspheroids than 2D-expanded-DPSC and CBD-treated microspheroids further induce osteogenic potential compared with CBD-treated 2D-expanded-DPSC.

DPSC microspheroids effectively translated in vitro CBD-stimulated osteoinductive effect during in situ bone regeneration

We prepared 2D-expanded DPSC and microspheroids loaded GelMA hydrogels construct for in vivo grafting as shown in Fig. 5A. We evaluated gross views of the constructs with 7.5×10^5 DPSC or 3×10^3 microspheroids (Fig. 5B). The live/dead cell double staining assays showed that the majority of DPSC and microspheroids in GelMA hydrogel constructs were viable at 1, 3 and 7 days. Similarly, DPSC in constructs gradually exhibited spindle shape fibroblastic morphology at day 7 (Fig. 5C). Therefore, our results showed that loading in GelMA hydrogel constructs did not affect the viability and morphology of DPSC and microspheroids.

To investigate in vitro osteoinductive stimulation translation ability of DPSC microspheroids during in situ bone regeneration, we established a nude mouse calvarial defect model. Micro-computed tomography (micro-CT) images revealed incomplete healing after 8 weeks in the 2D-expanded DPSC group. While CBD-treated 2D-expanded-DPSC and microspheroids groups significantly increased bone healing in the cranial defect model. In contrast, the CBD-treated microspheroids group exhibited the most abundant bone formation, and small peninsulas of bone nodule formation along the margins of bone defect could be observed (Fig. 6A). In addition, quantification of micro-CT images (Fig. 6B) provided further evidence that bone volume/total volume (BV/TV), bone surface/total volume (BS/TV), bone mineral density (BMD), trabecular thickness (Tb.Th) and trabecular number (Tb.N) were the highest and the trabecular separation (Tb.Sp) was the lowest in the CBD-treated microspheroids group compared with other groups tested.

To assess whether CBD and microspheroids improved new bone formation, the calvarial bone specimens were histologically analyzed. HE staining showed that new bone formation was limited, and only minimal new bone formation around the margins of the native bone in the DPSC group and CBD-treated DPSC group, where soft fibrous tissue filled the center of the defect area (Fig. 6C). Whereas a moderate and abundant amount of new bone was observed in the microspheroids and CBD-treated microspheroids group, which is statistically presented in Supplementary Fig. 2B. Furthermore, Masson's trichrome staining revealed that CBD-treated microspheroids formed the greatest amount of osteoid, with woven/lamellar features in the defect area, as compared with the other groups at 8 weeks (Fig. 6D). Our results showed that CBD-treated microspheroids induce abundant mineralized bone tissue formation and promote DPSC-based bone defect healing.

The induced osteogenic potential of CBD-treated microspheroids was attributed to WNT6 upregulation

We conducted mRNA-seq on DPSC and microspheroids with or without CBD after successive osteogenic induction for 14 days. A pairwise comparison was implemented to determine the expression difference. First, principal component analysis (PCA) showed data independence between the four groups, indicating the comparability of data (Supplementary Fig. 3A). The volcano plots revealed a large number of differentially expressed genes (DEGs) between the DPSC and microspheroids with or without CBD (Supplementary Fig. 3B). Microspheroids showed 1171 differentially upregulated and 861 differentially downregulated genes compared with DPSC. CBD-treated microspheroids showed 1513 differentially upregulated and 1454 differentially downregulated genes compared with CBD-treated DPSC. There were 1574 common DEGs during the analysis of overlapping DEGs in DPSC and microspheroids vs. CBD-treated DPSC (Fig. 7A). Kyoto Encyclopedia of Genes and Genomes (KEGG) pathway enrichment analysis of spheroids treated with and without CBD and these 1574 common DEGs revealed that the majority of DEGs enriched to osteogenesis-related WNT signaling pathway (Fig. 7B). The heatmap of WNT signaling related DEGs are shown Fig. 7C. Among these genes, WNT6 was upregulated 10-fold in CBD-treated microspheroids compared

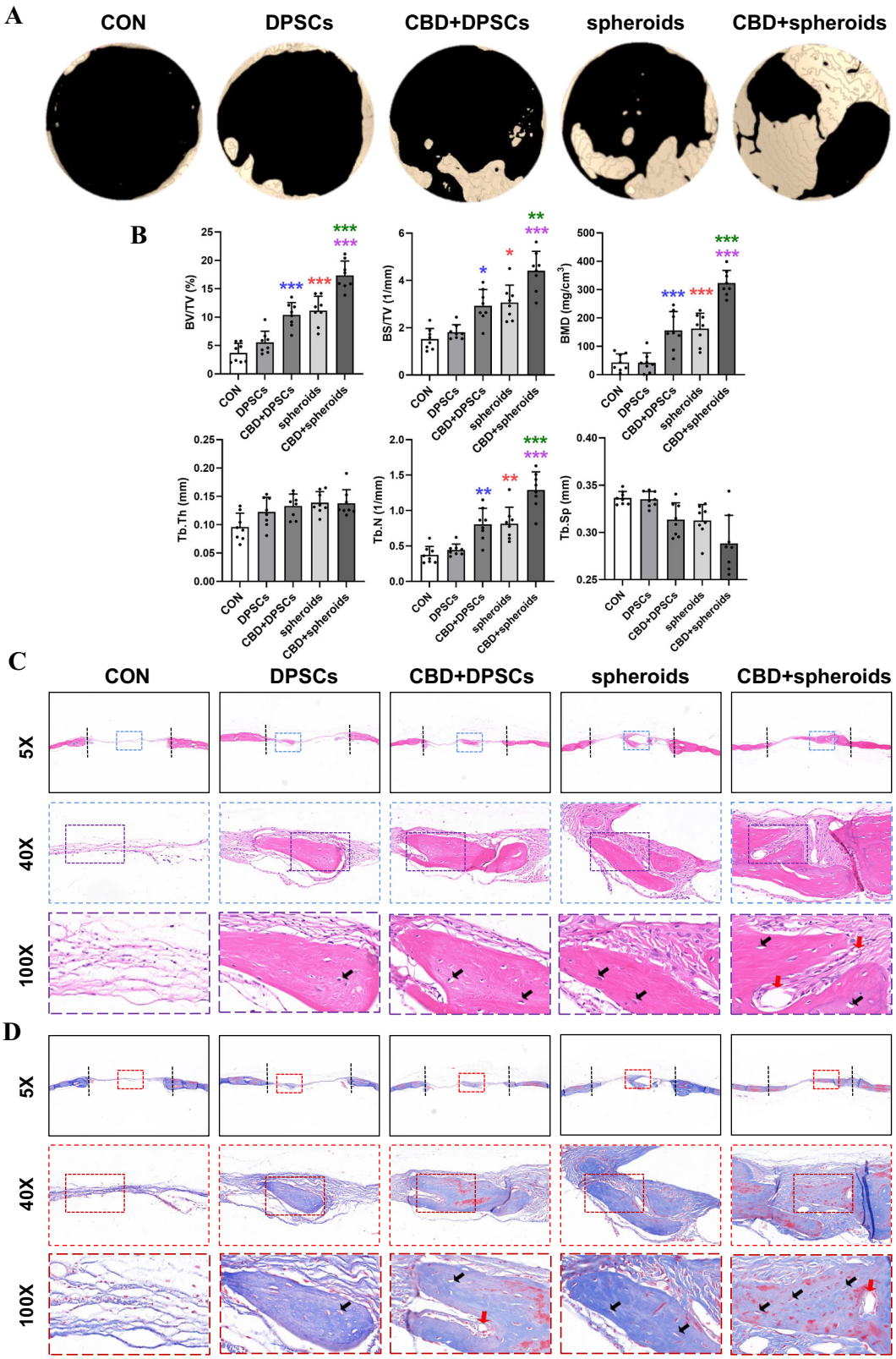

Fig. 6 | CBD-treated microspheroids promoted bone regeneration in mice calvarial bone defects. A Micro-CT images of calvarial bone defects after 8 weeks. **B** Quantitative analysis of newly formed bone parameters, bone volume/total volume (BV/TV), bone surface/total volume (BS/TV), bone mineral density (BMD), trabecular thickness (Tb.Th), trabecular number (Tb.N) and trabecular separation (Tb.Sp) ($n = 8$). Representative microscopic images of histological tissue sections: **C** HE staining and **D** Masson staining. Osteoblast (yellow arrows); Vessel (red arrows). Significant difference compared different groups, $^{*}P < 0.05$, $^{**}P < 0.01$, and $^{***}P < 0.001$; compared between DPSC and CBD+DPSC groups in blue; compared between DPSC and spheroids groups in red; compared between spheroids and CBD +spheroids groups in green; compared between CBD+DPSC and CBD+spheroids groups in purple.

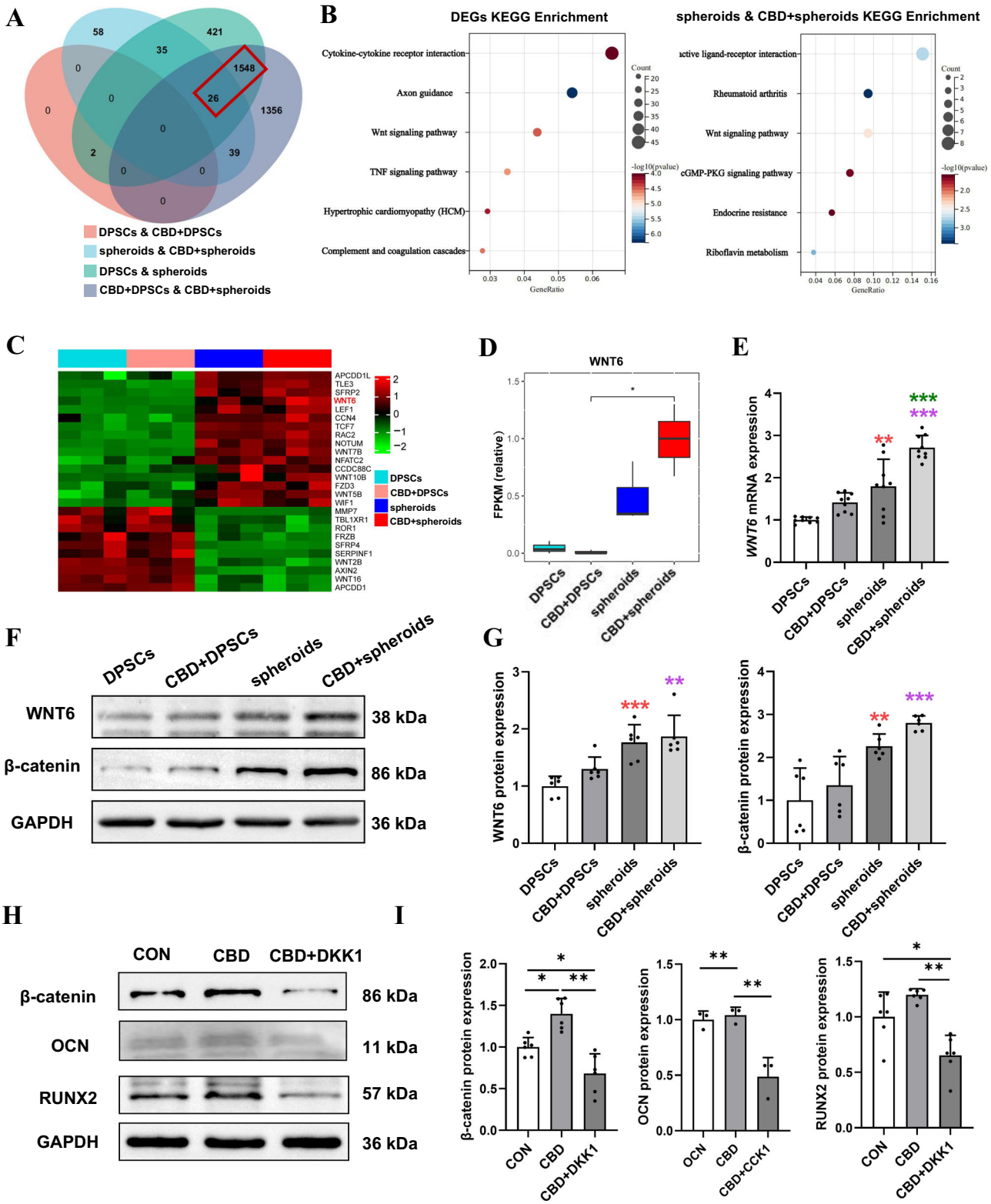

Fig. 7 | Transcriptomic analysis of DPSC and microspheroids with or without CBD treatment. A Venn diagram showing the differentially expressed genes (DGEs) between four groups. **B** KEGG analysis of common DEGs. **C** Heatmap displaying the Wnt/β-catenin pathway-related DGEs between DPSC and microspheroids with or without CBD. **D** Quantification of differentially expressed WNT6 analyzed based on FPKM. **E** mRNA expression of WNT6. **F** Western blot analysis of WNT6, β-catenin, and quantification (**G**). **H** Western blot analysis of β-catenin, OCN and RUNX2 protein expression of microspheroids upon DKK1 treatment for 48 h and quantification (**I**). Data were presented as the mean ± SD ($n = 3$). Significant difference compared different groups, $^{*}P < 0.05$, $^{**}P < 0.01$, and $^{***}P < 0.001$; compared between DPSC and CBD+DPSC groups in blue; compared between DPSC and spheroids groups in red; compared between spheroids and CBD +spheroids groups in green; compared between CBD+DPSC and CBD+spheroids groups in purple.

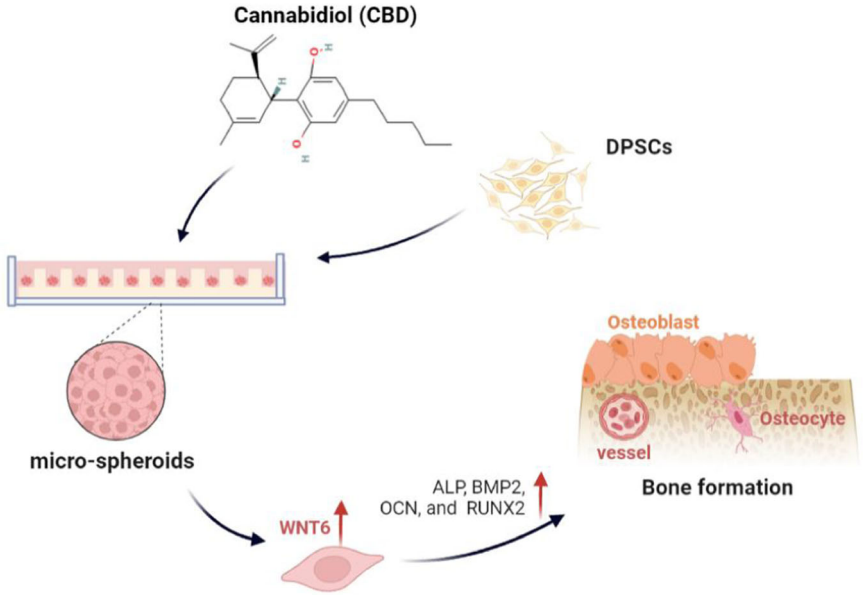

Fig. 8 | CBD-treated microspheroids promoted bone regeneration via WNT6. Schematic presentation of CBD-treated microspheroids and their osteogenic potential.

with CBD-treated DPSC (Fig. 7D). β-catenin, the downstream signaling of WNT6, is a key pathway involved in osteogenesis. We validated the expression pattern of WNT6 and β-catenin in DPSC and microspheroids with or without CBD treatment by RT-qPCR and Western blot analysis. (Fig. 7E–G and Supplementary Fig. 4B).

Dickkopf-related protein 1 (DKK1), a pharmacological inhibitor of the Wnt/β-catenin pathway, inhibits β-catenin formation by binding to the low-density lipoprotein receptor-related protein 5/6 component of the WNT receptor complex. Thus, we incubate CBD-treated microspheroids with or without additional DKK1 to further confirm the role of WNT6 in the higher osteogenic potential of CBD-treated microspheroids. Western blot analysis showed that DKK1 significantly downregulated the expression of β-catenin in CBD-treated microspheroids. Moreover, DKK1 also decreased the protein expression of OCN and RUNX2 (Fig. 7H, I and Supplementary Fig. 4C). These observations implied that CBD upregulates WNT6 in microspheroids that promote osteogenic potential via Wnt/β-catenin signaling.

Discussion

Cost-effective novel bone regeneration approaches are in urgent need for the effective repair of critical-sized bone defects. Although state-of-the-art stem cell therapy might be a potent tool for bone regeneration, the seed cell suspension cannot adequately represent the natural environment of stem cells in the body, such as tissue structure and cell–cell and cell–extracellular environment interactions[36]. Stem cell 3D construct better maintains desired cellular characteristics for tissue regeneration compared with conventional 2D-expanded cells[15]. Exogenous biomaterial-free, self-assembled, biomimetic, and injectable stem cell microspheroids are in urgent demand for bone regeneration applications. This study developed self-assembled DPSC microspheroids (≈70 μm diameter) with robust osteogenic differentiation potential and in situ bone regenerative potential. Moreover, DPSC microspheroids effectively translate in vitro CBD-induced osteoinductive effect during bone defect healing (Fig. 8). WNT6, a member of Wnt/β-catenin signaling was highly upregulated in the CBD-treated DPSC microspheroids, suggesting a potential role of Wnt/β-catenin signaling in CBD-treated DPSC microspheroid-mediated bone regeneration.

In this study, DPSCs were obtained from the dental pulp of premolars extracted for orthodontics treatment without an additional invasion[4]. We have further confirmed that DPSCs have common features of MSCs including colony formation and multilineage differentiation potential. A previous study reported that DPSCs are characterized by a rapid proliferation rate, high clonogenic potential, and ability to differentiate into distinct cell lineages including odontoblasts, osteoblasts, chondrocytes, and others[37]. In addition, DPSCs have been proven to induce bone tissue regeneration in the calvarial bone defect model[38]. Our results indicate that DPSCs isolated in this study are highly pure MSCs and can be used as a source of seed cells for bone tissue engineering applications.

Shreds of literature have reported that CBD promotes the osteogenic differentiation of MSCs from different sources including DPSC[39–41]. Some clinical studies have shown that CBD promotes the healing of non-infectious arthritis[42] and exerts a beneficial effect on bone metabolism[43]. In the present study, we found that CBD at a concentration of 0.1–2.5 μM did not inhibit the viability of DPSC but at a concentration of 12.5 μM dramatically inhibited the viability of DPSC. CBD (2.5 μM) robustly promoted the osteogenic differentiation of DPSC. These results are in agreement with other studies that a low dose of CBD (<10 μM) enhances the proliferation and osteogenic differentiation of MSCs[44–46], while the pro-mitotic effects weakened with a higher dose of CBD (>10 μM)[47–49]. Based on our findings, we choose CBD (2.5 μM) as an optimal concentration to induce osteogenic potential in microspheroids.

A stem cell 3D constructs simulate the in situ microenvironments of cells and retain the original biological characteristics of stem cells[26,36]. DPSC cell aggregates successfully regenerate dental pulp in clinics but 2D-expanded DPSC fails to do so[50]. Scaffold-free cell-aggregate culture techniques such as cell sheet aggregates, hanging drop microplates, magnetic levitation, and hydrogel-based spheroid culture fail to control the spheroid size and cell numbers/spheorids[51–53]. The large size of spheroids causes cell necrosis in the spheroid center and makes it difficult to uniformly load spheroids in microporous bone grafts. The use of hydrogel or biomaterial-based stem cell spheroids increases the exogenous biomaterial-based adverse effect in vivo. To address these issues, we developed biomaterial-free, self-assembled, biomimetic, and injectable DPSC microspheroids for the first time using the microwell culture technique[26]. In these intact microspheroids (≈70 μm diameter), DPSCs were well-compacted in a self-produced extracellular matrix mimicking organoid-like properties. A previous study had developed human periosteum stem cells-derived cartilaginous microspheroids to repair the critical-sized bone defect[26]. Our study directly developed osteogenic microspheroids from DPSC for bone regeneration applications. Our culture system avoids the use of growth factors that reduce the cost and eliminates the possible adverse effects carried by microspheroids due to the effect of those growth factors[26].

Although MSCs showed robust osteogenic potential in vitro, these cells fail to regenerate bone during in vivo transplantation[3]. This mainly occurs

due to the poor viability of cells in avascular bone grafts[54]. DPSC microspheroids grafted in bone defect showed higher bone regeneration potential compared with DPSC. This outcome is in accordance with the results from the previous studies using cell aggregates or spheroid[26]. Although the CBD-treated DPSC showed a better effect on bone regeneration compared to DPSC, this effect was not as pronounced as that of CBD-treated DPSC microspheroids. Our results indicated that microspheroids effectively translate the effect of CBD-induced in vitro osteoinductive stimulation during in situ bone regeneration. Although BMP2 has a robust bone regenerative potential, it has certain adverse effects during in vivo applications including ectopic bone regeneration postoperative inflammation and associated adverse effects, ectopic bone formation, osteoclast-mediated bone resorption, inappropriate adipogenesis, and cervical spine swelling[55,56]. Therefore, our developed DPSC microspheroids can be used as a BMP2/other osteogenic drug's effect carrier without direct application of these drugs in vivo. Such an approach eliminates the in vivo adverse effect of the directly applied drugs and simplifies the clinical translation of various osteogenic drugs.

The Wnt/β-catenin pathway regulates the cell fate of MSCs differentiating to osteoblasts[57,58]. A previous study indicated that WNT6 significantly enhanced β-catenin activity during osteogenic differentiation[59,60]. CBD-mediated rescue of bone loss, oxidative stress, and inflammation are mainly attributed to the activation of the Wnt/β-catenin pathway[61,62]. In this study, we took advantage of RNA-Seq to explore the differentiation of mechanisms in DPSC and microspheroids with or without CBD treatment and found that WNT6 was a key component upregulated and responsible for higher osteogenic potential of CBD-treated microspheroids. Inhibition of WNT6 signaling by DKK1 reduced the osteogenic potential of CBD-treated microspheroids. These results indicate the key role of WNT6 in the induced osteogenic potential of CBD-treated microspheroids. However, the mechanism of CBD-induced WNT6 activation in DPSC microspheroids should be further investigated. This study developed a self-assembled CBD-treated osteogenic DPSC microspheroids with activated WNT6 which indicate a promising bone regeneration application in clinics.

In this study, DPSC microspheroids with robust osteogenic potential were successfully cultured. These microspheroids not only promoted bone defect healing but also remarkably translated the effect of CBD-induced in vitro osteoinductive stimulation during in situ bone regeneration, indicating the application potential of DPSC microspheroids during bone defect reconstruction in clinics.

Methods

Isolation and characterization of DPSC

The present study was approved by the Medical Ethical Committee of the Affiliated Stomatology Hospital of Guangzhou Medical University (No. JCYJ2022021), and all patients signed an informed consent form. The DPSC were all obtained from the human pulp tissue of premolars that were removed for orthodontic treatment in the Affiliated Stomatology Hospital of Guangzhou Medical University. A total of 30 teeth from 20 patients (10 male, 10, female, 1–2 tooth/patient) were used for DPSC isolation. The inclusion criteria for teeth collection were the permanent teeth from 18- to 25-year-old patients without caries, periodontal disease, periapical lesion, and systemic inflammatory diseases. After extraction, the teeth surface was washed with phosphate-buffered saline (PBS) (Gibco, USA) containing 4% penicillin/streptomycin (Gibco, USA) two times. The pulp tissues were gently separated from the root and crown within 4 h, minced with sterile scissors into 1–2 mm fragments, then digested with 3 mg/mL collagenase type I (Gibco, USA) and 4 mg/mL dispase (Gibco, USA) for 45 min at 37 °C, and centrifuged at 1000 rpm for 5 min. The cells' precipitation was resuspended using alpha-modified minimal essential media (α-MEM; Gibco, USA) containing 15% fetal bovine serum (FBS) (Gibco, USA) and 1% penicillin/streptomycin, and cultured at 37 °C in an environment with 5% CO_2 with the medium replacement every 3 days. Upon reaching 80–90% confluency, cells were collected with 0.25% trypsin-EDTA (Gibco, USA) and subcultured at a 1:3 ratio. DPSC between passages 2 to 5 were used in subsequent experiments.

Flow cytometry analysis of DPSC surface markers

The DPSC of P3 in T75 flasks were digested with 0.25% trypsin-EDTA, collected, and incubated for 30 min with monoclonal antibodies against human CD29, CD34, CD44, CD45, CD73, CD90, and CD105 (BD Pharmingen, USA; Abcam, USA), as well as isotype-matched control IgG1. CD44 and CD105 were labeled with phycoerythrin (PE). CD45 and CD90 were labeled with PE-Cy5 conjugate. CD29, CD34, and CD73 were labeled with fluorescein isothiocyanate (FITC). The expression profiles for the cell surface markers were analyzed using a flow cytometer and Cell Quest software (Beckman Coulter, USA).

Colony-forming unit assay

Using the low-density cell seeding method, the capacity of colony-forming units was assessed. DPSC (P3) were seeded at a density of 500 cells/well into 6-well plates (Corning Incorporated, Corning, NY, USA) and maintained in the normal growth medium. After 7 days, cells were fixed with 4% paraformaldehyde for 10 min, washed twice with PBS, and stained with crystal violet staining (Sigma, USA).

Multilineage differentiation of DPSC

Alizarin red staining. DPSC (P3) were seeded in 6-well culture plates at a density of 10^5 cells/well and cultured in α-MEM supplemented with 10% FBS and 1% of penicillin/streptomycin at 37 °C with 5% CO_2 in a humidified incubator. When the cells became 80% confluence, the culture medium was replaced with osteogenic medium (growth medium supplemented with 10 mM beta-glycerophosphate, 50 mg/L ascorbic acid, and 10 nM dexamethasone). The osteogenic medium was replenished every 3 days. At day 21, the cells were fixed with 4% paraformaldehyde for 20 min at room temperature and washed with PBS. Osteogenic cultures were stained with 2% alizarin red solution, pH 4.2 (500 μL/well, Sigma-Aldrich), for 5–10 min to assess for mineral nodule deposition detection by light microscopy.

Oil red O staining. DPSC (P3) were seeded in 6-well culture plates at a density of 10^5 cells/well and cultured in α-MEM supplemented with 10% FBS and 1% of penicillin/streptomycin at 37 °C with 5% CO_2 in a humidified incubator. When the cells became 90% confluence, the culture medium was replaced with adipogenic medium (growth medium containing 10 mg/L insulin, 1 μM dexamethasone, 0.5 mM 3-Isobutyl-1-methylxanthine and 0.2 mM indomethacin). The adipogenic medium was replenished every 3 days. At day 28, the cells were fixed with 4% paraformaldehyde for 30 min at room temperature and washed with PBS. Adipogenic cultures were stained with a working solution of the Oil Red O staining (Solarbio, China) for 30 min to observe the formation of intracellular lipid vacuoles by light microscopy.

Alcian blue staining. DPSC (P3) were resuspended in a growth medium at a density of 4×10^6 cells/mL. Ten microliters of this cell suspension containing 4×10^4 cells were pipetted in the center of each well of a 48-well plate (Corning Incorporated, Corning, NY, USA). Then, micromasses were given 2 h to form. After that, maintenance medium (0.5 mL/well) was added for 1 day, followed by the addition of chondrogenic medium (growth medium supplemented with 50 mg/L ascorbic acid, 0.1 μM dexamethasone, 40 mg/L L-Proline, 10 μg/L TGF-β3, and 1% Insulin-Transferrin-Selenium). The chondrogenic medium was refreshed every 3 days. At day 21, the micro-masses were fixed with 4% paraformaldehyde for 30 min at room temperature and washed with PBS. Chondrogenic cultures were stained with a working solution of Alcian blue staining (Solarbio, China) for 30 min to assess the chondrogenic differentiation.

Cell proliferation assay

To determine the effect of CBD on DPSC proliferation ability, we used cell counting kit-8 (CCK-8; Dojindo, Japan). DPSC were seeded at a density of 2×10^3 cells/well in 96-well plates (Corning Incorporated, Corning, NY, USA) in triplicate. After 24 h of culture, the old medium was replaced with the medium containing 0, 0.1, 0.5, 2.5, and 12.5 μM CBD (Sigma, USA) respectively (six repeats per concentration). The medium was replaced every 3 days. At 1, 3, or 5 days, the culture medium was discarded. Then, the combination of 90 μL medium and 10 μL CCK8 reagent was added to each well and incubated in the incubator at 37 °C for 1 h. The results were recorded by a microplate reader (Thermofisher, USA) at an absorbance of 450 nm.

ALP staining and activity

DPSC (2×10^4 cells/well) were seeded in 48-well culture plates, and cultured in a complete medium for 24 h. Then, the old medium was replaced with the osteogenic medium containing 0, 0.1, 0.5, and 2.5 μM CBD respectively (four repeats per concentration). The medium was replenished every 3 days. On days 4 and 7, the original medium was removed. For ALP staining, the cells were fixed with 4% paraformaldehyde for 30 min. Then, the cells were washed twice with PBS and stained using the BCIP/NBT ALP color development kit (Beyotime, China). Staining was observed under a bright-field microscope. (Leica, Germany).

For the measurement of ALP activity, the cells were washed twice with PBS, and lysate was extracted in a lysis buffer containing 0.1% Triton X-100. The total protein concentration in the cell lysate was analyzed by the BCA protein assay kit (Thermo Scientific, USA). The activity of ALP was performed using the ALP assay kit (Nanjing Jiancheng Chemical Industrial Ltd, China). The results were measured by a microplate reader at an absorbance of 520 nm. The value of ALP activity was normalized to total protein content.

Matrix mineralization assays

DPSC (2×10^4 cells/well) were seeded in 48-well culture plates, and cultured in a complete medium for 24 h. Then, the old medium was replaced with the osteogenic medium containing 0, 0.1, 0.5, and 2.5 μM CBD respectively. The medium was replenished every 3 days. On day 21, the original medium was removed. The mineralized matrix was stained by alizarin red staining. For semiquantitative analysis of 150 μL of 10% cetylpyridinium chloride (CPC) solution (Sigma, USA), the solution was added to each well of 48-well culture plates to dissolve the mineralized nodules. The eluted liquid was transferred to the 96-well plates. The results were measured by a microplate reader at an absorbance of 562 nm.

Development of microspheroids and characterization

The PDMS master mold with 200 μm pillar diameter, 150 μm pillar height, and 100 μm gap between two neighboring pillars was fabricated and used to develop agarose-gel microwells for microspheroids culture. The PDMS mold was sterilized with 75% alcohol or under an ultraviolet lamp for 30 min. Agarose gel (Baygene, China; 3% w/v, agarose/deionized water) was sterilized using an autoclave and poured onto a PDMS mold containing pillars with a diameter of 200 μm. After allowing the agarose to solidify, microwell inserts with an area of ≈1.8 cm^2 were punched out and inserted in 24-well plates. PBS (1 mL) was then added, and the wells were sterilized using a UV light for 30 min. Each 24-well insert contained ≈2000 microwells. To form a microspheroid structure, DPSC were trypsinized, and 5×10^5 cells were diluted in 500 μL of serum-free chemically defined medium (iCell bioscience, China) and seeded in 24-well plates. Around 250 cells homed in each well and self-aggregated to form microspheroid. Microspheroids were further cultured in a serum-free osteogenic medium with or without CBD (2.5 μM). After that, images of microspheroids were captured at each time point, and the medium was changed every 48 h. For mechanism-related rescue experiments, CBD-treated microspheroids were incubated with an additional Wnt inhibitor (100 ng/mL recombinant DKK1, Sino biological, China) for 7 days. The half medium was replaced with fresh conditioned medium containing DKK1 every 24 h.

Live/dead staining

Cell viability in microspheres was assessed qualitatively with the Live/Dead viability/cytotoxicity kit (Solarbio, China). Briefly, microspheroids were rinsed with PBS, whereafter they were incubated in 2×10^{-6} M Calcein-AM and 4×10^{-6} M Propidium Iodide for 30 min at 37 °C, 5% CO_2, and 95% humidity. Images of each stained microspheroids were captured on days 1, 3, 7, and 14 using confocal laser scanning microscopy (CLSM, Leica TCS SP8). Live cells stain green and dead cells stain red.

Staining for cytoskeleton

Microspheroids were fixed for 30 min at room temperature with 4% paraformaldehyde, rinsed with PBS, permeabilized for 30 min with PBS containing 0.5% Triton X-100, and rinsed with PBS. Cell nucleus and F-actin distribution within microspheroids were visualized by staining with DAPI (Solarbio, China) and 0.8 U/mL TRITC conjugated Phalloidin (Solarbio, China) for 1 h at room temperature. Sequential images of the microspheroids were captured using CLSM using respective filters. The Leica AF image processing software was used to construct 3D images.

RT-qPCR analysis

Total RNA was extracted from DPSC and microspheroids using an RNA isolation kit (Accurate Biotechnology, China). The total RNA (500 ng) from each sample was reverse-transcribed to cDNA (Accurate Biotechnology, Hunan, China). RT-qPCR was performed using an SYBR Green RT-qPCR kit (Accurate Biotechnology, Hunan, China). The gene expressions of osteogenic markers ALP, BMP2, RUNX2, OPN, OCN, and WNT6 were analyzed by RT-qPCR. The data were normalized to the internal control GAPDH. The primer sequences used for RT-qPCR are listed in Table 1.

Western blotting

DPSC and microspheroids were lysed with RIPA buffer (Beyotime, China) containing protease inhibitors (PMSF; Beyotime, China) on ice for 30 min. The cell lysate was centrifuged at 12,000 rpm for 15 min to collect the supernatant. Total protein concentration was measured using the BCA protein assay kit (Thermo Scientific, USA). Total protein (20 μg) was loaded in 10% SDS-PAGE gel (Epizyme, China) for protein separation and transferred into polyvinylidene fluoride (PVDF) membranes (Millipore, Billerica, MA, USA) using wet blotting techniques. The membrane was blocked with 5% nonfat milk powder for 1 h and washed thrice with TBST. The membrane was then incubated at 4 °C overnight with primary antibodies, which included rabbit anti-ALP (Affinity, China), rabbit anti-BMP2 (Abcam, England), rabbit anti-OCN (Abcam, England), rabbit anti-human Collagen I (COL-I, Abcam, England), rabbit anti-human RUNX2 (Abcam, England), rabbit anti-human WNT6 (Bioss, China), and rabbit anti-human β-catenin (Bioss, China). After incubation, the primary antibodies were removed. Horseradish peroxidase (HRP)-conjugated secondary antibody (Abcam, England) was incubated at room temperature for 1 h. The protein bands were detected using an enhanced chemical luminescence kit (Beyotime, China). The ImageJ software was used for the semi-quantification of band intensity.

Preparation of GelMA hydrogels constructs

GelMA (EFL-GM-60) was purchased from Engineering For Life, Hangzhou, China. Following the manufacturer's instructions, a 0.05 g initiator was mixed with 20 mL PBS and dissolved in water at 45 °C to prepare a 0.25% (w/v) initiator standard solution. GelMA (2 g) was added to the initiator standard solution at 65 °C and mixed for 20–30 min to get 10% (w/v) GelMA hydrogel. Finally, the GelMA hydrogel was sterilized by filtering through a 0.22 μm syringe filter.

Before implantation, both DPSC and microspheroids were cultured in an osteogenic medium with or without CBD for 2 weeks. Then, 2D-

Table 1 | Primers used in RT-qPCR to examine gene expression

Gene	Acc. No	Primer sequence (5′-3′)	Product length (bp)
ALP	NM_001127501.4	F: GGACCATTCCCACGTCTTCAC R: CCTTGTAGCCAGGCCCATTG	137
BMP2	NM_001200.4	F: GGGAGAAGGAGGAGGCAAAGA R: CTGGGGAAGCAGCAACGCTA	190
RUNX2	NM_001015051.4	F: ACCCAGAAGGCACAGACAGAAG R: AGGAATGCGCCCTAAATCACT	82
OCN	NM_199173.5	F: CTCACACTCCTCGCCCTATTGG R: GTAGCGCCTGGGTCTCTTCACT	147
OPN	NM_000582.2	F: GCTAAACCCTGACCCATC R: CTTTCGTTGGACTTACTTGG	72
COL-I	NM_000088.4	F: CAGTGGTAGGTGATGTTCTGGGAG R: CAAGAGGCATGTCTGGTTCGG	150
WNT6	NM_006522.4	F: GTGCAACTGCACAACAACGAGG R: GAAATGGAGGCAGCTTCTGCCA	127
GAPDH	NM_001357943.2	F: GGACCTGACCTGCCGTCTAG R: GTAGCCCAGGATGCCCTTGA	100

expanded DPSCs were digested with 0.25% trypsin-EDTA. Microspheroids or 2D-expanded DPSC have resuspended in 10% (w/v) GelMA hydrogels. Microspheroids or 2D-expanded DPSC-loaded GelMA constructs (≈7.5×10^5 DPSC/3×10^3 microspheroids per construct, $n = 8$) with a diameter of 3 mm and a depth of 1 mm were exposed to LAP 405 nm blue light (Engineering For Life, China) for 5 s. DPSC and microspheroids constructs were cultured at 37 °C incubator with 5% CO_2 before implantation. To assess cell viability, the Live/Dead staining assay was performed on the GelMA hydrogel constructs cultured in vitro for 1, 3, and 7 days.

Mice calvarial bone defect repair

The 40 cranial defects were randomly separated into five groups: (1) control, (2) DPSC, (3) CBD (2.5 μM)-treated DPSC, (4) microspheroids, and (5) CBD (2.5 μM)-treated microspheroids. Controls were transplanted with 10% (w/v) GelMA hydrogel constructs.

Animal experiments were conducted following the protocols approved by the Laboratory Animal Ethics Committee of Guangdong Huawei Testing Co., LTD in this study (No.20220103). Forty male athymic nude mice (Zhuhai BesTest Bio-Tech Co., Ltd., China), 6–8 weeks old and weighing 19–26 g were used. Animals were housed at a specific pathogen-free animal facility in stable conditions (22 ± 2 °C) with a 12 h dark/light cycle and ad libitum access to food and water. Animals were allowed to acclimatize for 1 week before experiments and were regularly monitored for signs of pain/infection, food intake, and activity during the entire experimental period.

Preoperatively, all animals were anesthetized by intramuscular injections of ketamine hydrochloride (35 mg/kg) and xylazine (5 mg/kg). Following anesthesia, the calvarial bone was exposed, and a 3 mm circular bone defect was created with a trephine drill under normal saline irrigation. Constructs were placed into the defect, and the skin was sutured to close the wound. The animals received antibiotic therapy for 3 days. After 8 weeks, the mice were sacrificed by isoflurane inhalation through the approved Ethics Committees' methods, and calvarial bone was collected and fixed with 4% paraformaldehyde for subsequent micro-CT and histological analysis.

Micro-CT analysis

Micro-CT images were taken using micro-CT equipment (Skyscan-1172; Bruker, Kontich, Belgium). The X-ray source is set at 60 kV and 100 μA the three-dimensional image is obtained by isotropy with the voxel size of 10 μm. The serial sections were reconstructed into a 3D image using reconstructions and osteogenic parameters conducted with NRecon v.1.6.9 software. CTAn (Bruker micro-CT, BE) was used for all image processing and quantification of mineralized tissue. The percentage of mineralized tissue was calculated with respect to the total explant volume. Bone volume was measured by using a fixed threshold setting for all images. CTvox (Bruker micro-CT, BE) was used to create 3D visualization. The osteogenic parameters such as BV/TV, BS/TV, BMD, Tb.Th, Tb.N and Tb.Sp were measured.

Histology and immunostaining analysis

For histological analysis, all samples were fixed, demineralized, dehydrated, and embedded in paraffin. The sample blocks were sectioned to a thickness of 4 μm and stained with hematoxylin and eosin (H&E) as well as Masson's trichrome. The newly formed bone area in H&E-stained tissue sections was measured using ImageJ software.

Microspheroids were fixed with 4% paraformaldehyde at room temperature for 2 h and washed with PBS. After centrifugation at 500 rpm for 5 min, microspheroids were snap-frozen, embedded in optimal cutting temperature (OCT) compound, and sectioned on a cryostat at 5-μm thickness. After blocking with 1% bovine serum albumin (BSA; Sigma-Aldrich) for 1 h at room temperature, the frozen sections were incubated with the primary antibodies OCN (1:500; Proteintech, China) overnight. After a washing step with PBS, the secondary antibody was applied for 1 h (CoraLite488-conjugated Goat Anti-Rabbit IgG, 1:200; Proteintech, China). After nuclear staining with DAPI, sample imaging was performed with CLSM. Immunofluorescence staining was quantified using ImageJ software from three different samples.

mRNA sequencing and bioinformatics analysis

The total RNA of DPSC and microspheres treated for 21 days with or without 2.5 μM CBD was extracted using Trizol® (Invitrogen, Carlsbad, CA). RNA samples were detected based on the A260/A280 absorbance ratio with a Nanodrop ND-2000 system (Thermo Scientific, USA), and the RIN of RNA was determined by an Agilent Bioanalyzer 4150 system (Agilent Technologies, CA, USA). Only qualified samples will be used for library construction. Paired-end libraries were prepared using an ABclonal mRNA-seq lib prep kit (ABclonal, China) following the manufacturer's instructions. PCR products were purified (AMPure XP system) and library quality was assessed on an Agilent Bioanalyzer 4150 system. Finally, the library preparations were sequenced on an MGISEQ-T7, and 150 bp paired-end reads were generated (Shanghai Applied Protein Technology, China). The data generated from the BGI platform were used for bioinformatics analysis. RNA-seq sequencing data quality was verified by Fastqc. Then clean reads were separately aligned to the reference genome with orientation mode using HISAT2 software to obtain mapped reads. FeatureCounts was used to count the reads numbers mapped to each gene. Fragments Per Kilobase per Million (FPKM) of each gene were calculated based on the length of the gene and the reads count mapped to this gene. Differential expression analysis for

mRNA was performed using R package edgeR. Differentially expressed RNAs with |log2(FC)| value >1 and q value <0.05, considered as significantly modulated, were retained for further analysis.

Statistics and reproducibility

All data were obtained from at least three independent experiments, with each experiment in triplicate under identical conditions, and shown as the mean ± standard deviation (SD). To test the significance of observed differences between the study groups, one-way analysis of variance (ANOVA) or Student's t-test of the GraphPad Prism Software (version 9.0, USA) was used. A value of $P < 0.05$ was considered a significant difference.

Reporting summary

Further information on research design is available in the Nature Portfolio Reporting Summary linked to this article.

Data availability

The data that support the findings of this study are available in the Supplementary Data file, and the uncropped and unedited blot/gel images are provided in Supplementary Fig. 4. All other data are available from the corresponding author on reasonable request. Source data underlying the graphs and charts in the main figures are provided as Supplementary Data 1.

Received: 13 February 2023; Accepted: 30 July 2024;
Published online: 10 August 2024

References

1. Chan, Y. H. et al. Melatonin enhances osteogenic differentiation of dental pulp mesenchymal stem cells by regulating MAPK pathways and promotes the efficiency of bone regeneration in calvarial bone defects. *Stem Cell Res. Ther.* **13**, 73 (2022).
2. Maroulakos, M. et al. Applications of 3D printing on craniofacial bone repair: a systematic review. *J. Dent.* **80**, 1–14 (2019).
3. Gugliandolo, A. et al. Oral bone tissue regeneration: mesenchymal stem cells, secretome, and biomaterials. *Int. J. Mol. Sci.* **22**, 5236 (2021).
4. Zhang, W. & Yelick, P. C. Tooth repair and regeneration: potential of dental stem cells. *Trends Mol. Med.* **27**, 501–511 (2021).
5. Kunimatsu, R. et al. Effects of human deciduous dental pulp-derived mesenchymal stem cell-derived conditioned medium on the metabolism of HUVECs, osteoblasts, and BMSCs. *Cells* **11**, 3222 (2022).
6. Bacakova, L. et al. Stem cells: their source, potency and use in regenerative therapies with focus on adipose-derived stem cells—a review. *Biotechnol. Adv.* **36**, 1111–1126 (2018).
7. Atlas, Y. et al. Microvascular maturation by mesenchymal stem cells in vitro improves blood perfusion in implanted tissue constructs. *Biomaterials* **268**, 120594 (2021).
8. Yang, X. et al. Stem cells from human exfoliated deciduous teeth as an alternative cell source in bio-root regeneration. *Theranostics* **9**, 2694–2711 (2019).
9. Gual-Vaques, P. et al. Autogenous teeth used for bone grafting: a systematic review. *Med. Oral Patol. Oral Cir. Bucal* **23**, e112–e119 (2018).
10. Cen, X. et al. miR-20a-5p contributes to osteogenic differentiation of human dental pulp stem cells by regulating BAMBI and activating the phosphorylation of Smad5 and p38. *Stem Cell Res. Ther.* **12**, 421 (2021).
11. Zheng, C. et al. Stem cell-based bone and dental regeneration: a view of microenvironmental modulation. *Int. J. Oral. Sci.* **11**, 23 (2019).
12. Walmsley, G. G. et al. Stem cells in bone regeneration. *Stem Cell Rev. Rep.* **12**, 524–529 (2016).
13. Yuan, Y. et al. Adipose-derived stromal/stem cells are verified to be potential seed candidates for bio-root regeneration in three-dimensional culture. *Stem Cell Res. Ther.* **13**, 234 (2022).
14. Zhang, S. et al. The effects of spheroid formation of adipose-derived stem cells in a microgravity bioreactor on stemness properties and therapeutic potential. *Biomaterials* **41**, 15–25 (2015).
15. Jiang, Z. et al. Genetically modified cell sheets in regenerative medicine and tissue engineering. *Biomaterials* **275**, 120908 (2021).
16. Futrega, K. et al. Spheroid coculture of hematopoietic stem/progenitor cells and monolayer expanded mesenchymal stem/stromal cells in polydimethylsiloxane microwells modestly improves in vitro hematopoietic stem/progenitor cell expansion. *Tissue Eng. Part C Methods* **23**, 200–218 (2017).
17. Xu, H. et al. Organoid technology and applications in cancer research. *J. Hematol. Oncol.* **11**, 116 (2018).
18. Bar-Ephraim, Y. E., Kretzschmar, K. & Clevers, H. Organoids in immunological research. *Nat. Rev. Immunol.* **20**, 279–293 (2020).
19. Regmi, S. et al. Enhanced viability and function of mesenchymal stromal cell spheroids is mediated via autophagy induction. *Autophagy* **17**, 2991–3010 (2021).
20. Cho, S. et al. Preclinical study of human bone marrow-derived mesenchymal stem cells using a 3-dimensional manufacturing setting for enhancing spinal fusion. *Stem Cells Transl. Med.* **11**, 1072–1088 (2022).
21. Petrenko, Y., Sykova, E. & Kubinova, S. The therapeutic potential of three-dimensional multipotent mesenchymal stromal cell spheroids. *Stem Cell Res. Ther.* **8**, 94 (2017).
22. Suarez-Martinez, E. et al. 3D and organoid culture in research: physiology, hereditary genetic diseases and cancer. *Cell Biosci.* **12**, 39 (2022).
23. Xu, X., Farach-Carson, M. C. & Jia, X. Three-dimensional in vitro tumor models for cancer research and drug evaluation. *Biotechnol. Adv.* **32**, 1256–1268 (2014).
24. Zhang, L. et al. Three-dimensional (3D) printed scaffold and material selection for bone repair. *Acta Biomater.* **84**, 16–33 (2019).
25. Bates, R. C., Edwards, N. S. & Yates, J. D. Spheroids and cell survival. *Crit. Rev. Oncol. Hematol.* **36**, 61–74 (2000).
26. Nilsson Hall, G. et al. Developmentally engineered callus organoid bioassemblies exhibit predictive in vivo long bone healing. *Adv. Sci.* **7**, 1902295 (2020).
27. Gao, Z. R. et al. Traditional Chinese medicine promotes bone regeneration in bone tissue engineering. *Chin. Med.* **17**, 86 (2022).
28. Zhang, Y., Ma, J. & Zhang, W. Berberine for bone regeneration: therapeutic potential and molecular mechanisms. *J. Ethnopharmacol.* **277**, 114249 (2021).
29. Kogan, N. M. et al. Cannabidiol, a major non-psychotropic cannabis constituent enhances fracture healing and stimulates lysyl hydroxylase activity in osteoblasts. *J. Bone Min. Res.* **30**, 1905–1913 (2015).
30. Blevins, L. K. et al. Evaluation of the anti-inflammatory effects of selected cannabinoids and terpenes from *Cannabis sativa* employing human primary leukocytes. *Food Chem. Toxicol.* **170**, 113458 (2022).
31. Casares, L. et al. Cannabidiol induces antioxidant pathways in keratinocytes by targeting BACH1. *Redox Biol.* **28**, 101321 (2020).
32. Muthumalage, T. & Rahman, I. Cannabidiol differentially regulates basal and LPS-induced inflammatory responses in macrophages, lung epithelial cells, and fibroblasts. *Toxicol. Appl. Pharm.* **382**, 114713 (2019).
33. Qi, X. et al. Investigation of in vitro odonto/osteogenic capacity of cannabidiol on human dental pulp cell. *J. Dent.* **109**, 103673 (2021).
34. Volmar, M. N. M. et al. Cannabidiol converts NF-kappaB into a tumor suppressor in glioblastoma with defined antioxidative properties. *Neuro Oncol.* **23**, 1898–1910 (2021).
35. Sarzi-Puttini, P. et al. Medical cannabis and cannabinoids in rheumatology: where are we now? *Expert Rev. Clin. Immunol.* **15**, 1019–1032 (2019).

36. Wu, X. et al. Recent advances in three-dimensional stem cell culture systems and applications. *Stem Cells Int.* **2021**, 9477332 (2021).
37. Nuti, N. et al. Multipotent differentiation of human dental pulp stem cells: a literature review. *Stem Cell Rev. Rep.* **12**, 511–523 (2016).
38. Lee, Y. C. et al. Comparing the osteogenic potentials and bone regeneration capacities of bone marrow and dental pulp mesenchymal stem cells in a rabbit calvarial bone defect model. *Int. J. Mol. Sci*. **20**, 5015 (2019).
39. Apostu, D. et al. Cannabinoids and bone regeneration. *Drug Metab. Rev.* **51**, 65–75 (2019).
40. Schmuhl, E. et al. Increase of mesenchymal stem cell migration by cannabidiol via activation of p42/44 MAPK. *Biochem. Pharm.* **87**, 489–501 (2014).
41. Luo, H. et al. Cannabidiol increases proliferation, migration, tubulogenesis, and integrity of human brain endothelial cells through TRPV2 activation. *Mol. Pharm.* **16**, 1312–1326 (2019).
42. Vela, J. et al. Cannabidiol treatment in hand osteoarthritis and psoriatic arthritis: a randomized, double-blind, placebo-controlled trial. *Pain* **163**, 1206–1214 (2022).
43. Heineman, J. T. et al. A randomized controlled trial of topical cannabidiol for the treatment of thumb basal joint arthritis. *J. Hand Surg. Am.* **47**, 611–620 (2022).
44. Miller, H. et al. Role of marijuana components on the regenerative ability of stem cells. *Cell Biochem. Funct.* **39**, 432–441 (2021).
45. Olivas-Aguirre, M. et al. Cannabidiol directly targets mitochondria and disturbs calcium homeostasis in acute lymphoblastic leukemia. *Cell Death Dis.* **10**, 779 (2019).
46. Kamali, A. et al. Cannabidiol-loaded microspheres incorporated into osteoconductive scaffold enhance mesenchymal stem cell recruitment and regeneration of critical-sized bone defects. *Mater. Sci. Eng. C Mater. Biol. Appl.* **101**, 64–75 (2019).
47. Solinas, M. et al. Cannabidiol inhibits angiogenesis by multiple mechanisms. *Br. J. Pharm.* **167**, 1218–1231 (2012).
48. Massi, P. et al. The non-psychoactive cannabidiol triggers caspase activation and oxidative stress in human glioma cells. *Cell Mol. Life Sci.* **63**, 2057–2066 (2006).
49. Nabissi, M. et al. Cannabidiol stimulates Aml-1a-dependent glial differentiation and inhibits glioma stem-like cells proliferation by inducing autophagy in a TRPV2-dependent manner. *Int. J. Cancer* **137**, 1855–1869 (2015).
50. Xuan, K. et al. Deciduous autologous tooth stem cells regenerate dental pulp after implantation into injured teeth. *Sci. Transl. Med.* **10**, eaaf3227 (2018).
51. Lee, S. et al. High-throughput formation and image-based analysis of basal-in mammary organoids in 384-well plates. *Sci. Rep.* **12**, 317 (2022).
52. Condello, I. Magnetic levitation pumps for cell-free hemoglobin prevention during VV ECMO. *Crit. Care* **26**, 86 (2022).
53. Jensen, C. & Teng, Y. Is it time to start transitioning from 2D to 3D cell culture? *Front. Mol. Biosci.* **7**, 33 (2020).
54. Le, H. et al. Mesenchymal stem cells for cartilage regeneration. *J. Tissue Eng.* **11**, 2041731420943839 (2020).
55. James, A. W. et al. A review of the clinical side effects of bone morphogenetic protein-2. *Tissue Eng. B Rev.* **22**, 284–297 (2016).
56. Nguyen, V. et al. BMP-2-induced bone formation and neural inflammation. *J. Orthop.* **14**, 252–256 (2017).
57. Zhang, L. et al. Overexpression of MiR-335-5p promotes bone formation and regeneration in mice. *J. Bone Min. Res.* **32**, 2466–2475 (2017).
58. Clevers, H. & Nusse, R. Wnt/beta-catenin signaling and disease. *Cell* **149**, 1192–1205 (2012).
59. Feng, L. et al. MicroRNA-378 suppressed osteogenesis of MSCs and impaired bone formation via inactivating Wnt/β-catenin signaling. *Mol. Ther. Nucleic Acids* **21**, 1017–1028 (2020).
60. Zheng, M. et al. Beta-tricalcium phosphate promotes osteogenic differentiation of bone marrow-derived mesenchymal stem cells through macrophages. *Biomed. Mater.* **16**, 025005 (2021).
61. Vallee, A., Vallee, J. N. & Lecarpentier, Y. Potential role of cannabidiol in Parkinson's disease by targeting the WNT/beta-catenin pathway, oxidative stress and inflammation. *Aging* **13**, 10796–10813 (2021).
62. Li, D. et al. Cannabidiol administration reduces sublesional cancellous bone loss in rats with severe spinal cord injury. *Eur. J. Pharm.* **809**, 13–19 (2017).

Acknowledgements

This study was supported by the National Key Research and Development Program of China (2021YFE0108000), the National Natural Science Foundation of China (82150410451), and the Guangzhou Science and Technology Plan Project (2023B03J1240). Figures 3B, 5A and 8 were created with BioRender.com.

Author contributions

F.L. conducted the experiments and obtained the results. F.L., Q.W., B.C. and X.L. sorted and analyzed the results; Q.L. and X.L. assisted with in vitro experiments; F.L., J.P. and N.W. wrote the draft. J.P. and J.L. extensively revised, formatted, and submitted versions of the manuscript. All authors participated in data discussions and approved the final version of the submission.

Competing interests

The authors declare no competing interests.

Additional information

Supplementary information The online version contains supplementary material available at https://doi.org/10.1038/s42003-024-06655-y.

Correspondence and requests for materials should be addressed to Janak L. Pathak or Jiang Li.

Peer review information *Communications Biology* thanks Sheng-Wei Feng, XiaoLei Li and the other anonymous reviewer(s) for their contribution to the peer review of this work. Primary handling editors: Eirini Trompouki and Manuel Breuer. A peer review file is available.